Thermal-diffusivity measurements of ultrahigh thermal conductors with use of scanning photothermal rate-window spectrometry: Chemical-vapor-deposition diamonds

Zhuohui Chen and Andreas Mandelis
Department of Mechanical Engineering, Photothermal and Optoelectronic Diagnostics Laboratory, University of Toronto, Toronto, Ontario, Canada M5S 1A4
and Ontario Laser and Lightwave Research Center, University of Toronto, Toronto, Ontario Canada M5S 1A4
(Received 1 June 1992)

A comprehensive study of a photothermal rate-window spectrometry for thermal-diffusivity measurements of ultrahigh thermal conductors, using either a dual-channel boxcar averager or a lock-in amplifier, is presented. Theoretical analysis of infrared radiometric transients and techniques to extract the diffusivities of materials from the transient are discussed. By exploiting the derivative signal nature of the rate-window methodology, one can measure the thermal diffusivity of the sample with superior signal-to-noise (S/N) ratio from the maximum position of the radiometric rate-window signal. Our measurements of thermal diffusivities of chemical-vapor-deposition diamonds made by the hot-filament process as a function of temperature between 60 and 300 K are the first such photothermal data obtained completely nonintrusively and they illustrate the unique potential of this measurement methodology for the nondestructive, noncontact photothermal investigation of ultrahigh thermal-conductor thermophysics, largely inaccessible by other diagnostic probes.

I. INTRODUCTION

In recent years with the development of technology in electronic materials and devices, a knowledge of thermophysical properties of these materials and devices has become increasingly important. Many techniques have been developed for measuring the thermal diffusivity, thermal conductivity, and heat capacity of materials.[1–16] Among these techniques, thermal waves have attracted widespread interest.[6–16] Due to the fact that thermal wave propagation depends on the thermal diffusivity of the material, one can measure this quantity from the frequency- and/or time-domain behavior of the thermal wave. Nevertheless, when a photothermal measurement in condensed matter with very high values of thermal transport properties is contemplated, such as diamond, there are stringent instrumental and background noise requirements to be satisfied before an acceptable measurement can be performed. These considerations tend to eliminate most conventional photothermal techniques from being suitable candidates.

In most cases, a thermal wave is generated by a laser beam at the surface of a solid or a film in a layered structure. One photothermal technique which has been found most suitable to measure the temperature variation of such ultrahigh thermal conductors uses the optical beam deflection caused by the mirage effect.[11–16] In this method, the surface is heated by a modulated laser beam. A probe laser beam skimming the sample surface is used to measure the variation of local temperature caused by the heating beam. The probe beam is deflected by the temperature gradient of the refractive index in the air or in any other surrounding fluid. From the mirage phase signal which is a function of the offset distance between the heating and probe beams, one can obtain the thermal diffusivity of the sample. This method requires not only a painstaking point-by-point measurement by changing the relative positions of the probe and pump laser beams, but also an empirical multiparameter routine for fitting the experimental data sets to the theoretical curve.[14–16] This makes the technique cumbersome and less straightforward for interpreting the data. In addition, mirage effect cryogenic temperature measurements in air may be difficult or impossible, due to the partial vacuum required in conventional experimental chambers. This restricts the utility of this technique to relatively high temperatures. Another remote-detection thermal wave technique suitable for the thermal-diffusivity measurement is photothermal radiometry (PTR).[6–10] This method can be used to measure thermal responses of materials in frequency and/or time domain. The heating source can be a short-duration laser pulse[8,10] or a modulated laser beam,[8,9] and the thermal radiation emitted from the sample surface is measured using an IR detector. The transients are recorded by using a digitizer in the case of pulsed heating, or the amplitude and phase signals are measured by using a lock-in amplifier. In both modes of the conventional PTR, a curve fitting procedure is needed to obtain the thermal diffusivity of the sample. Moreover, both the conventional frequency-domain PTR and mirage effect techniques encounter another problem when one measures very thin films or ultrahigh thermal conductors,

especially very thin diamond films:[17] Diamond has the highest thermal conductivity of any known material at room temperature. Because of the thinness of the film and the large thermal diffusivity, the thermal transit time constant of diamond thin films is very small, and therefore frequencies over 1 MHz are required in the measurement. This poses two kinds of problems. The highest frequency available from commercial lock-in amplifiers is only up to 120 kHz–1 MHz, and the rapid attenuation of the frequency-domain thermal wave signal makes the measurement very difficult in the high-frequency range. An alternative approach to circumvent the high-frequency requirements is to measure the effect of heat propagation parallel to the surface.[17–19] Even with this improved method, however, the measurement could not be extended beyond 200 Hz because of the high attenuation of the thermal wave.[17]

Other non-thermal-wave techniques have also been adopted in measuring the thermal parameters of conventional materials. By measuring the temperature distribution along the length of the sample which is suspended in vacuum between two heated supports by means of a thermograph, the thermal conductivity of the sample can be obtained from a solution of the steady-state heat diffusion equation.[20] A more conventional steady-state four-probe technique is also used to measure the thermal conductivity.[21] Thermocouples are attached to a strip of delaminated film and one end of the film is heated to establish a thermal current in the sample. The thermal conductivity is then calculated from a measurement of the temperature at two points along the film. These methods are not only cumbersome but also require a fair amount of sample preparation and are intrusive (contacting). They may be very inefficient for measurements in ultrahigh thermal conductors of certain geometries.

With dramatically increased requirements for fast and efficient heat sinking in computer memories and very large scale integrated (VLSI) device technology, ultrahigh thermal conductors such as diamond have become valuable candidates for such applications. For the characterization of their thermophysical properties *in situ*, a rapid, sensitive, nonintrusive, and noncontact methodology for the measurement of thermal transport is required. In this paper, we present a new technique, scanning photothermal rate-window spectrometry, for the transient photothermal signal generation and analysis. The concept of "rate window" was introduced in conjunction with deep-level transient spectroscopy (DLTS), which is widely used in the semiconductor industry to measure deep impurity levels in semiconductor materials.[22–24] Boxcar photothermal rate-window spectrometry, as recently introduced by Mandelis and Chen,[25] combines the simplicity of interpretation of time-domain measurements and the high-precision measurement feature of the rate-window extremum. No curve fitting procedure is involved. The method involves a kind of derivative signal approach, and thus has advantages over the conventional photothermal methods in view of its better sensitivity to the thermophysical properties of materials.[26] When using a lock-in amplifier to set up the rate window, the technique exhibits, in addition, superior signal-to-noise (S/N) ratio even in low-temperature ranges, which makes feasible for the first time the reliable noncontact measurement of thermophysical properties of ultrahigh thermal conductors at cryogenic temperatures. It will be shown in this work that lock-in photothermal rate-window spectrometry combines the advantages of the straightforward interpretation of fast time-domain photothermal detection with the high S/N ratio characteristic of narrow-band frequency-domain signals, and is, therefore, optimally suited for studies of the thermophysics of ultrahigh thermal conductors, such as diamonds.

Our photothermal rate-window spectrometry system consists of a heat source from a low-fluence cw, acousto-optically pulsed laser beam, an infrared radiometric system for the transient measurement, and a dual-channel boxcar averager or a lock-in amplifier to set the rate window. The cw acousto-optically pulsed laser has an advantage over a Q-switched pulsed laser, the latter being likely to cause non-negligible thermal perturbations to the sample. For measuring the temperature dependence of the thermophysical properties, a variable temperature cryostat is employed. The maximum on the resulting rate-window signal, which is a function of pulse period, is used to obtain the characteristic time constant of the transient. Therefore, for a sample with known thickness, it can be used to measure the thermal diffusivity. For a material with known thermal diffusivity, it is possible to use the technique to monitor in real time the thickness of a film during the growth process.

In Sec. II we present the appropriate theory of the time-domain infrared photothermal radiometry of coated transparent solids. The experimental system and chemical-vapor-deposition (CVD) diamond samples used in this work are described in Sec. III. In Sec. IV we discuss two scanning photothermal rate-window spectrometries with the experimental results from the CVD diamond samples. In Sec. V we discuss the temperature dependence of thermal conductivity of the CVD diamonds and in Sec. VI we give a comparison of the two photothermal rate-window spectrometries (boxcar averager and lock-in amplifier). Finally in Sec. VII we briefly summarize the main results of the paper.

II. INFRARED RADIOMETRIC TRANSIENTS

Scanning photothermal rate-window spectrometry is a technique for measuring thermal properties from transient signals from a sample. In order to conduct the analysis, one must first measure the thermal transients of the sample. Photothermal radiometry is a well-known method in the study of thermal[7–10] and electronic[27–29] properties of solid materials in a nondestructive and noncontact fashion, and it has been widely used with great success in the analysis of a wide range of materials from composites to ion-implanted semiconductor wafers. In this section, we discuss the theoretical aspects of the time-domain measurement using infrared photothermal radiometry with a solid sample geometry representative of our CVD surface-coated diamond samples.

A. Thermal diffusion

In what follows, we assume a one-dimensional model for the heat flow in a gas-solid-gas system, shown in Fig. 1. The heat flow resulting from the absorbed light energy from an excitation laser pulse of duration τ_p, and the evolution of temperature inside the sample, is governed by the thermal diffusion equations. In the Laplace transform domain

$$\frac{d^2\tilde{T}_g(x,s)}{dx^2}-\frac{s}{\alpha_g}\tilde{T}_g(x,s)=0\ ,\quad x\le 0\ , \tag{1a}$$

$$\frac{d^2\tilde{T}_s(x,s)}{dx^2}-\frac{s}{\alpha_s}\tilde{T}_s(x,s)=0\ ,\quad 0\le x\le L\ , \tag{1b}$$

$$\frac{d^2\tilde{T}_g(x,s)}{dx^2}-\frac{s}{\alpha_g}\tilde{T}_g(x,s)=0\ ,\quad x\ge L\ . \tag{1c}$$

$\tilde{T}_j$ is the Laplace transform of the photothermally induced temperature increase in region j [$j=g$ (gas) or s (solid)]. α_j is the respective thermal diffusivity, and s is the Laplace variable. The temperature $\tilde{T}_s(x,s)$ is the Laplace transform of the solution in the solid, subject to the heat-flux conservation boundary conditions

$$-\kappa_s\frac{d\tilde{T}_s(0,s)}{dx}+\kappa_g\frac{d\tilde{T}_g(0,s)}{dx}=Q_1H(s)\ , \tag{2a}$$

$$-\kappa_s\frac{d\tilde{T}_s(L,s)}{dx}+\kappa_g\frac{d\tilde{T}_g(L,s)}{dx}=Q_2H(s)\ , \tag{2b}$$

and temperature continuity conditions

$$\tilde{T}_s(0,s)=\tilde{T}_g(0,s)\ , \tag{3a}$$

$$\tilde{T}_s(L,s)=\tilde{T}_g(L,s)\ , \tag{3b}$$

where

$$H(s)=\frac{1-e^{-s\tau_p}}{s}\ , \tag{4}$$

and Q_1 and Q_2 are the heat fluxes at the front and rear surfaces, respectively. For samples like metals, the entire optical energy is absorbed at the front surface, where it is converted nonradiatively into heat, therefore $Q_1=\eta I_0$, $Q_2=0$. For samples which are transparent at the wavelength of the excitation beam, for instance, CVD diamonds [transparent in the wavelength range between 220 and 2500 nm (Ref. 30)], thin coatings are employed to absorb the optical energy at the surfaces (Fig. 2). In this case, and neglecting higher-order reflections at the interfaces

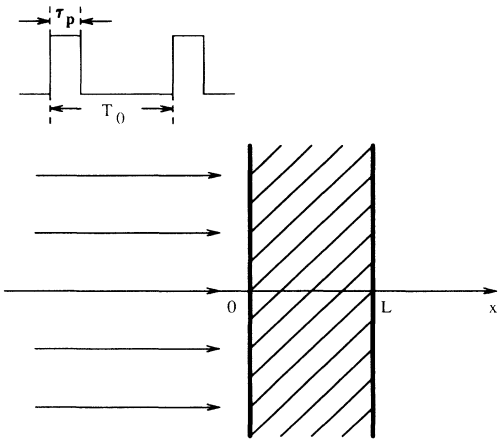

FIG. 1. Schematic of the infrared radiometry of a thin solid slab in a one-dimensional heat flow model.

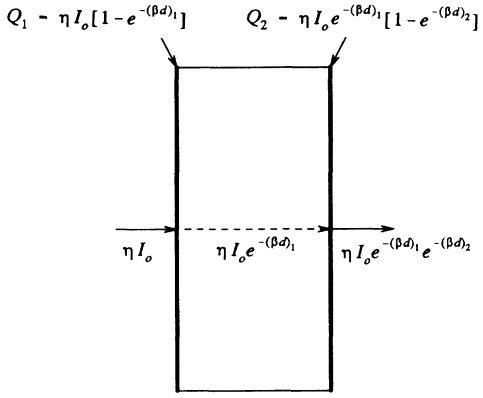

FIG. 2. Schematic of transparent sample with absorption coatings on both surfaces. Multiple internal reflections were ignored.

$$Q_1=\eta I_0[1-e^{-(\beta d)_1}]\ , \tag{5a}$$

$$Q_2=\eta I_0 e^{-(\beta d)_1}[1-e^{-(\beta d)_2}]\ . \tag{5b}$$

In this work, the coatings at both sides of the sample are the same, therefore approximately $(\beta d)_1=(\beta d)_2$.

Assuming solutions $\tilde{T}_g(x,s)$ and $\tilde{T}_s(x,s)$ in the form

$$\tilde{T}_g(x,s)=c_1(s)e^{a_g x}\ ,\quad x\le 0\ , \tag{6a}$$

$$\tilde{T}_s(x,s)=c_2(s)e^{-a_s x}+c_3(s)e^{a_s x}\ ,\quad 0\le x\le L\ , \tag{6b}$$

$$\tilde{T}_g(x,s)=c_4(s)e^{-a_g(x-L)}\ ,\quad x\ge L\ , \tag{6c}$$

and substituting Eqs. (6) into (1)–(3), the general expression for $\tilde{T}_s(x,s)$ is obtained:

$$\tilde{T}_s(x,s)=\frac{Q_1H(s)}{\kappa_s a_s}\frac{1}{e^{a_sL}-e^{-a_sL}}\times\left[\left[e^{a_sL}-\frac{Q_2}{Q_1}\right]e^{-a_sx}+\left[e^{-a_sL}-\frac{Q_2}{Q_1}\right]e^{a_sx}\right]\ . \tag{7}$$

B. Photothermal radiometric signal

Once we find the Laplace transform of the temperature distributions inside the sample, $\tilde{T}_s(x,s)$, we can calculate the transform of the thermal radiation signal $\tilde{S}_B(s)$ for materials with no additional thermal relaxation effects (such as electron-hole recombination lifetimes in semiconductors), using a generalized form of Stefan's law[9]

$$\tilde{S}_B(s)=K\beta'\int_0^L \tilde{T}_s(x,s)e^{-\beta' d}dx$$
$$=K\beta'\left\{\frac{c_2(s)}{\beta'+a_s}[1-e^{-(\beta'+a_s)L}]+\frac{c_3(s)}{\beta'-a_s}[1-e^{-(\beta'-a_s)L}]\right\}, \quad (8)$$

where $K=\epsilon\sigma T_a^3$ is a constant. Assuming the sample is optically opaque at the IR emission wavelength bandwidth of the infrared detector ($\beta' L \gg 1$), when $t \gg 1/\alpha_s\beta'^2$, the transform of the backscattered radiometric signal can then be written as

$$\tilde{S}_B(s)\simeq K[c_2(s)+c_3(s)]$$
$$=\frac{KQ_1(\alpha_s)^{1/2}}{\kappa_s}(1-e^{-s\tau_p})\sum_{n=0}^{\infty}\left\{\frac{e^{-2nL\sqrt{s}/(\alpha_s)^{1/2}}}{s^{3/2}}+\frac{e^{-2(n+1)L\sqrt{s}/(\alpha_s)^{1/2}}}{s^{3/2}}-2\frac{Q_2}{Q_1}\frac{e^{-2(n+0.5)L\sqrt{s}/(\alpha_s)^{1/2}}}{s^{3/2}}\right\}. \quad (9)$$

Inverting the expression for $\tilde{S}_B(s)$, one obtains the evolution of the time-dependent backscattered radiometric signal

$$S_B(t)=\begin{cases}J(t), & t\le\tau_p\\ J(t)-J(t-\tau_p), & t\ge\tau_p,\end{cases} \quad (10)$$

where

$$J(t)=2KQ_1\frac{(\alpha_s)^{1/2}}{\kappa_s}\sum_{n=0}^{\infty}\sqrt{t}\left\{i\,\mathrm{erfc}\left[n\pi\left[\frac{\tau_\alpha}{t}\right]^{1/2}\right]+i\,\mathrm{erfc}\left[(n+1)\pi\left[\frac{\tau_\alpha}{t}\right]^{1/2}\right]-2\frac{Q_2}{Q_1}i\,\mathrm{erfc}\left[(n+\tfrac{1}{2})\pi\left[\frac{\tau_\alpha}{t}\right]^{1/2}\right]\right\} \quad (11)$$

and

$$i\,\mathrm{erfc}(x)=\frac{1}{\sqrt{\pi}}e^{-x^2}-x\,\mathrm{erfc}(x). \quad (12)$$

Equation (11) shows that the radiometric signal depends upon the thermal characteristic time constant $\tau_\alpha=L^2/\pi\alpha_s$ and the surface coating absorptance βd. Furthermore, the decay portion of the radiometric signal depends also on the excitation pulse duration τ_p.

In Eq. (11) the first term on the right-hand side represents the thermal wave components traveling into the bulk of the sample, the second term represents the thermal wave components reflected from the back surface of the sample. The third term is the effect of the optical energy absorbed at the rear surface and it plays an important role in the measurement. It does not represent an independent heating source, but a portion of the optical flux "leaked" past the front surface. The extra thermal source at the rear surface slows down the thermal decay. The smaller the βd of the surface coating, the smaller the portion of heat energy absorbed at the front surface, and therefore the stronger the heat source at the rear surface. In the case where the entire optical energy is absorbed at the front surface, $Q_2=0$.

For a semi-infinite sample, only the first term with $n=0$ on the right-hand side of Eq. (11) is not zero. Therefore Eq. (11) becomes

$$S_B(t)=2KQ_1\frac{(\alpha_s)^{1/2}}{\kappa_s}\begin{cases}\sqrt{t}, & t\le\tau_p\\ \sqrt{t}-\sqrt{t-\tau_p}, & t\ge\tau_p.\end{cases} \quad (13)$$

The thermal properties (α_s and κ_s) of the sample affect only the amplitude of the transient, and one cannot extract thermal transport information from the thermal decay.

Figure 3 shows theoretical profiles of infrared radiometric signals with various characteristic time constants τ_α. The transients with different time constants overlap for $t \ll \tau_\alpha$ because the thermal energy has not yet reached the rear surface of the sample (thermally thick condition). The smaller the time constant τ_α, the earlier the transient becomes flat. This can be explained by the fact that the sample with a smaller time constant will attain the steady state faster.

It is worthwhile pointing out that the thermal transient eventually decays to zero after staying flat for a while. Because of the heat-flux continuity boundary condition used in our theoretical model, the thermal energy absorbed by the sample leaks to the surrounding air. The

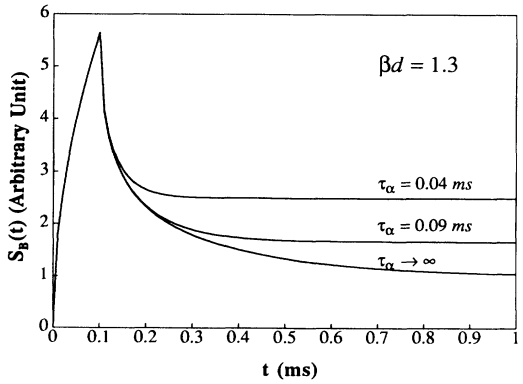

FIG. 3. Theoretical profiles of infrared radiometric signal showing the effect of characteristic time constant τ_α with pulse duration $\tau_p=0.1$ ms.

flat region in the transient represents the temporary thermal equilibrium inside the sample, which is tantamount to adiabatic boundary conditions.[10]

III. EXPERIMENTAL SYSTEM AND CVD DIAMOND SAMPLES

Figure 4 shows the experimental arrangement of the photothermal radiometry for time-domain measurements. A pulsed laser beam obtained by modulating a cw Ar^+-ion laser using an acousto-optic modulator was slightly focused on the sample surface at the size of approximately 1 mm diameter so as to preserve the one dimensionality of the problem. The resulting infrared radiation emitted from the sample surface was collected by two off-axis paraboloidal mirrors and detected using a liquid-N_2-cooled cadmium-mercury-telluride detector. According to the method for setting up a rate window, the transient was then directed to a lock-in amplifier for scanning photothermal lock-in rate-window spectrometry, or to a boxcar averager (or a digitizer to save the transients in the computer memory and using the computer to play the role of the boxcar averager) for scanning photothermal boxcar rate-window spectrometry. Details for setting up the rate window will be presented in the following section. For the measurement of the temperature dependence of thermal conductivity, the CVD diamond samples used in this work were suspended in a cryostat. A thermocouple was attached to the edge of the sample for the measurement of ambient temperature and a ZnSe window was used for the infrared measurement.

The diamond samples used in this work were fabricated at General Electric Research Laboratories, Schenectady, N.Y. The two CVD diamonds, designated D-1 and D-2, were made by the "hot-filament" process in which the depositing carbon is stabilized by bathing it in a flux of atomic hydrogen produced by dissociating molecular hydrogen over a tungsten filament. The thicknesses of the two samples were 240 and 741 μm, respectively. They were cut into 7-mm-diameter disks and both sides had been coated with 3000 Å of a chromium-based alloy. The absorptance βd of the coating was found to be 1.3. Although no further characterization of the diamond crystals was performed prior to the photothermal measurements, the samples were known to consist of inhomogeneous, non-uniform size crystal structure with the smallest crystal grain boundaries on the side of the probed surface (the side where crystal growth was initiated).

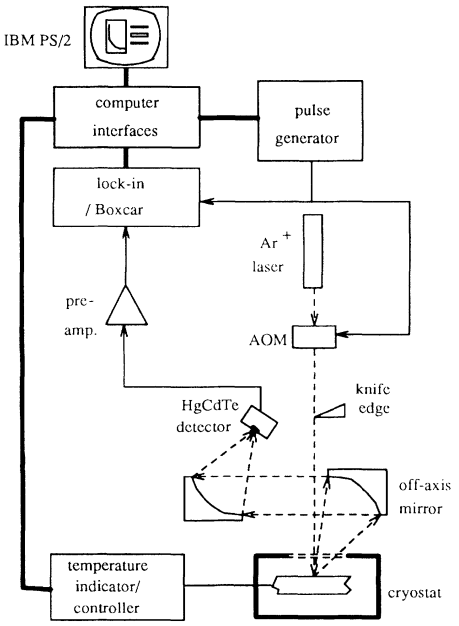

FIG. 4. Experimental system of photothermal rate-window spectrometry.

IV. SCANNING PHOTOTHERMAL RATE-WINDOW METHODOLOGIES

The thermophysical properties inherent in the thermal transients can always be extracted from the shape of the transient, i.e., by fitting the experimental transients with the theoretical prediction. Another technique to extract the information from the transient is to use the rate-window method. It is well established that any linear filtering operation is equivalent to an integral transformation.[24] The output signal $e_{\text{out}}(t,T_0)$ of a linear filter responding to a transient input signal $e_{\text{in}}(t,\tau)$ can be determined by a periodic reference signal $e_{\text{RW}}(t,T_0)$, which establishes the rate windows, i.e.,

$$e_{\text{out}}(\tau_\alpha,T_0)=\frac{1}{T_0}\int_0^{T_0} e_{\text{in}}(t,\tau_\alpha)e_{\text{RW}}(t,T_0)dt \ , \qquad (14)$$

where T_0 is the period of the reference signal. The integration represents the correlation between the physics of the input transient signal (characteristic time constant τ_α) and the instrumentally established rate window (the weighting function). Since the output signal $e_{\text{out}}(\tau_\alpha,T_0)$

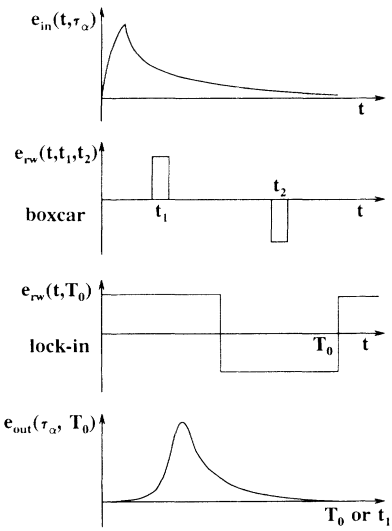

FIG. 5. Thermal transient, weighting functions, and rate-window output signal schematic.

is related to τ_α and T_0, one can expect a maximum from the output signal by varying either τ_α (e.g., varying the input signal by varying the temperature) or T_0 (varying the setting of the rate window). Thus, from the position of the maximum of the output signal, one can find the characteristic time constant and therefore obtain the material information related to the time constant. Since the time constant τ_α of a thermal relaxation is determined by the thermal diffusivity and the thickness of the sample as shown in the preceding section, we can measure the thermal diffusivity of the sample from the time constant τ_α obtained from the peak position of the output by varying the rate window. This is the basic idea of the thermal rate-window spectrometry.

There are several means of establishing a rate window, as shown in Fig. 5. In the use of a double boxcar to select the rate window, we fix the ratio t_2/t_1, and vary both t_1 and t_2 accordingly.[22,25,26] By plotting the output signal against t_1, one can identify the maximum position $(t_1)_{\max}$. In this work we also use a lock-in amplifier in the rate-window setup.[23,25] By varying the period (or frequency) of the reference signal, which is also the period (or frequency) of the repetitive excitation pulse, one then obtains a similar output signal as in the photothermal boxcar rate-window spectrometry, but with the advantage of the superior S/N ratio afforded by the narrowband spectral filtering of the lock-in analyzer.

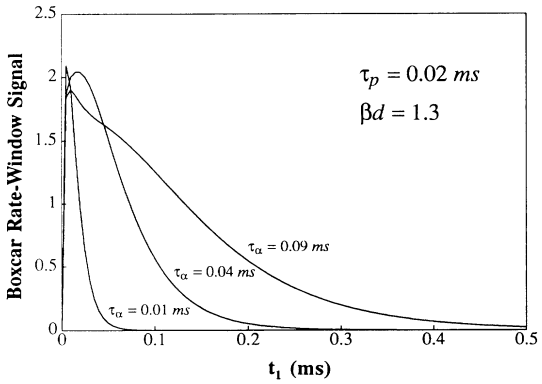

(a)

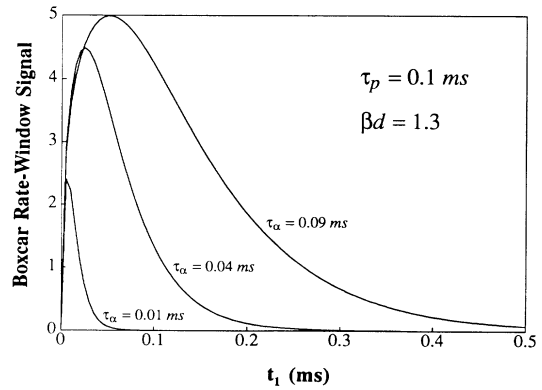

(b)

FIG. 6. Theoretical photothermal boxcar rate-window signals for various characteristic time constant with $t_2/t_1=2$ and $\beta d=1.3$. (a) $\tau_p=0.02$ ms. (b) $\tau_p=0.1$ ms.

A. Scanning photothermal boxcar rate-window spectrometry

Figure 6 shows theoretical photothermal boxcar rate-window signals for samples with various characteristic time constants. The calculation was performed by substituting the thermal transient of Eq. (10) and the proper rate-window function of the boxcar averager into Eq. (14). In Fig. 6(a) the pulse duration is 0.02 ms, and in Fig. 6(b) the duration is 0.1 ms. The longer the time constant τ_α, the later time the maximum of the rate-window signal appears. Figure 6 also shows clearly the effects of the pulse duration τ_p on the measurement. For samples with the same time constant τ_α, the longer the pulse duration τ_p, the later the maximum will appear, because the longer heat supply from regions deeper into the solid will slow down the thermal decay.

The positions of the maxima in Fig. 6 are found numerically from the partial derivative $\partial e_{\text{out}}/\partial t_1=0$ in Eq. (14). Figure 7 shows the maximum position $(t_1)_{\max}$ of the photothermal boxcar rate-window signal versus time constant of the samples for various surface absorption conditions. The pulse duration used in the calculation is 0.02 ms.

There are several important aspects in Fig. 7. First, the absorptance of the surface coating plays an important role in the measurement. In the case of $\beta d \to \infty$, which is the case when all the optical energy is absorbed at the front surface, the arrangement can only measure the time constant up to 0.025 ms before signal saturation. For finite βd, there is a maximum in the curve. For $\beta d=1.3$, the measurement of the time constant can extend to 0.042 ms and for $\beta d=1.0$, the measurement can extend to 0.055 ms. The smaller the βd, the larger the portion of heating energy transmitted by the front surface, and therefore thermal waves from deeper positions in the bulk can contribute more significantly to the time evolution of the front surface PTR transient response. For this reason a surface coating with small βd can be used to measure a sample with long time constant.

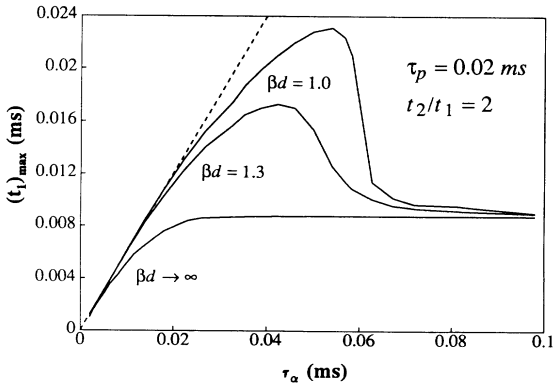

FIG. 7. Boxcar rate-window maximum $(t_1)_{\max}$ vs characteristic time constant τ_α for various surface absorption conditions. $\tau_p=0.02$ ms.

In the range of τ_α from 0 to τ_p, the relation between the maximum position $(t_1)_{\max}$ and the time constant τ_α is almost linear:

$$(t_1)_{\max} \cong 0.6\tau_\alpha \text{ (ms)} \quad \text{for } \tau_\alpha \in [0, \tau_p] \tag{15}$$

as shown in Fig. 7 in dashed line. A 1% change in the time constant of a material causes roughly 0.6% shift in the maximum position of the rate-window signal. The maximum position is very sensitive to the time constant τ_α of the sample, and therefore sensitive to the thermal diffusivity. The sensitivity of $(t_1)_{\max}$ to the time constant depends on the ratio t_2/t_1. The larger the ratio, the less sensitive $(t_1)_{\max}$ is to the time constant. Utilizing this feature, the technique can be used to measure small changes in time constant caused by the temperature, sample thickness, or impurities in condensed phase materials. For time constant longer than the pulse duration, the relation between $(t_1)_{\max}$ and the time constant becomes nonlinear.

For samples with time constant longer than a certain value ($\tau_\alpha > 0.1$ ms for partial absorption at the front surface; $\tau_\alpha > 0.025$ ms for total absorption the front surface), the curves become flat and converge to the same saturation value. As a result the maximum positions are no longer sensitive to the changes in time constant. These are the cases of very thick samples or samples with very small thermal diffusivity. Basically these kinds of samples are semi-infinite solids from the point of view of thermal waves. As discussed in the preceding section, thermal properties of a semi-infinite sample, which are only included in the amplitude of a thermal transient, do not affect the details of the decay of the thermal transient. Consistently with Fig. 7 and from Eq. (13), the thermal decay of a semi-infinite sample only depends on the pulse duration. It is found empirically that the relation between $(t_1)_{\max}$ and pulse duration τ_p for a semi-infinite sample is linear

$$(t_1)_{\max} \simeq 0.4362\tau_p \text{ (ms)} \quad \text{for } t_2/t_1 = 2 \text{ , } L \to \infty \text{ .} \tag{16}$$

The larger the ratio t_2/t_1, the smaller the slope of the $(t_1)_{\max}$ vs τ_α curve.

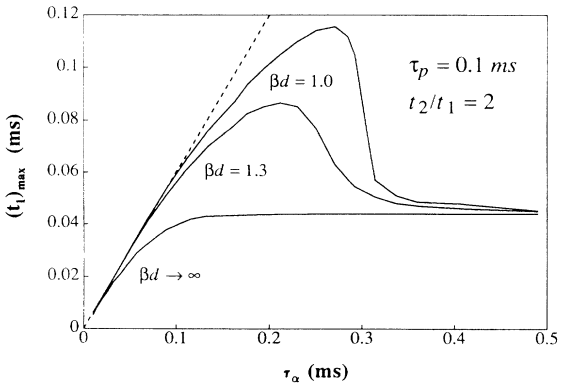

FIG. 8. Boxcar rate-window maximum $(t_1)_{\max}$ vs characteristic time constant τ_α for various surface absorption conditions. $\tau_p = 0.1$ ms.

From the above discussion it becomes clear that the technique is ideally suitable for the measurement of thin films or materials with large thermal diffusivities. For thick samples or samples with very small thermal diffusivity, on the other hand, one can increase the duration of heating pulse to perform the measurement. For this case, the locus of maximum position $(t_1)_{\max}$ of the photothermal boxcar rate-window signal with pulse duration 0.1 ms is shown in Fig. 8. In the range of τ_α from 0 to τ_p, Eq. (14) is valid. It can be seen from the curves that because of the longer pulse duration, the measurement range of time constants increases above that of Fig. 7. For $\beta d = 1.0$, the technique can measure accurately the time constant up to 0.275 ms and for $\beta d = 1.3$, up to 0.210 ms which are 5 times larger than the range shown in Fig. 7 with pulse duration of 0.02 ms. In fact, the range of time constant which can be measured increases linearly with pulse duration.

Figure 9(a) is the infrared photothermal radiometric transient of the diamond sample D-1. The duration of the heating pulse is 0.02 ms. Because of the short pulse duration, the heating energy is very small, and as a consequence the transient shown in Fig. 9(a) is very noisy. Figure 9(b) shows the boxcar rate-window signal which is calculated from the smoothed transient signal. From the $(t_1)_{\max}$ of 8.1 μs one can readily obtain the diffusivity of 4.47 cm^2/s using Fig. 7 (curve $\beta d = 1.3$). The solid line in Fig. 9(a) shows the theoretical result calculated by substituting this value of thermal diffusivity into Eq. (10). Thermal conductivity κ can be calculated by using the definition $\alpha = \kappa/\rho C$ and assuming the bulk values for the density ρ and heat capacity C. Using handbook values[31] for ρ and C the corresponding thermal conductivity κ is then found to be 8.02 W cm^{-1} K^{-1}, a value more representative of polycrystalline diamond[32] rather than a single crystal. This result is consistent with the nonuniform growth history of our sample.

A longer pulse duration not only extends the measurements of time constant, but also increases the S/N ratio of transient signals. Figure 10(a) is the transient obtained

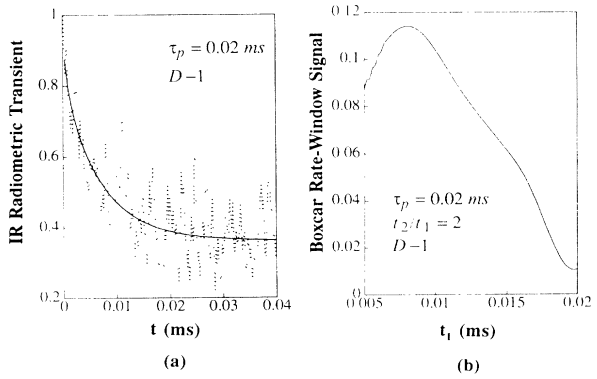

FIG. 9. Backscattered IR radiometric transient (a) and its boxcar rate-window signal (b) of a CVD diamond D-1; $L = 240$ μm, $\tau_p = 0.02$ ms, and $t_2/t_1 = 2$. The solid line is the theoretical calculation by substituting the measured thermal diffusivity into Eq. (10). Only the decaying part of the thermal response is shown following the end of the optical pulse.

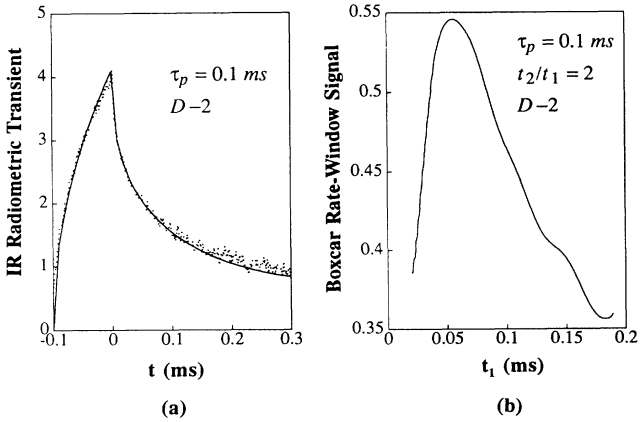

FIG. 10. Backscattered IR radiometric transient (a) and its boxcar rate-window signal (b) of a CVD diamond D-2; $L = 741$ μm, $\tau_p = 0.1$ ms, and $t_2/t_1 = 2$. The solid line is the theoretical calculation by substituting the measured thermal diffusivity into Eq. (10).

from the other CVD diamond sample D-2. Compared to the transient in Fig. 9(a), this transient is more clear. Figure 10(b) is the corresponding boxcar rate-window signal with maximum position $(t_1)_{\max}$ at 61 μs. The calculated thermal diffusivity and thermal conductivity are then found to be 4.93 cm^2/s and 8.85 $W\,cm^{-1}\,K^{-1}$, respectively.

The room-temperature thermal conductivities of the CVD diamonds are comparable with the value of 8.7 $W\,cm^{-1}\,K^{-1}$ for a 0.45-mm-thick hot-filament CVD diamond sample,[17] but smaller than the values for the diamond samples grown by the microwave plasma-enhanced CVD process.[19] A comparison of the thermal conductivity values at room temperature from this work and some earlier studies on CVD diamond films is given in Table I.

B. Photothermal lock-in rate-window spectrometry

The lock-in amplifier is a popular instrument for measuring a modulated signal, but it can also be used to measure a transient signal. If the time constant τ_L of the lock-in amplifier is much longer than the period T_0 of the repetitive input transient signal, which is also the period of the lock-in reference, the output of the lock-in amplifier will be the fundamental Fourier component of the transient.[25,33] The Fourier expansion of the input transient $e_{\rm in}(t)$ over the interval $0 \le t \le T_0$ is

$$e_{\rm in}(t) = \frac{a_0}{2} + \sum_{n=1}^{\infty} \left[a_n \cos\left[\frac{2\pi n}{T_0} t \right] + b_n \sin\left[\frac{2\pi n}{T_0} t \right] \right] \tag{17a}$$

or

$$e_{\rm in}(t) = \frac{a_0}{2} + \sum_{n=1}^{\infty} c_n \sin\left[\frac{2\pi n}{T_0} t + \phi_n \right] , \tag{17b}$$

where

$$a_n = \frac{2}{T_0} \int_0^{T_0} e_{\rm in}(t) \cos\left[\frac{2\pi n}{T_0} t \right] dt , \tag{18a}$$

$$b_n = \frac{2}{T_0} \int_0^{T_0} e_{\rm in}(t) \sin\left[\frac{2\pi n}{T_0} t \right] dt , \tag{18b}$$

and

$$c_n = (a_n^2 + b_n^2)^{1/2} \tag{19a}$$

with

$$\phi_n = \tan^{-1}\left[\frac{b_n}{a_n} \right] . \tag{19b}$$

The amplitude signal from a dual-channel lock-in amplifier measures the amplitude of the fundamental Fourier component c_1, while the lock-in phase signal corresponds to the phase ϕ_1 of the input transient, provided that $t_\theta = 0$ and $T_r = T_0$ in Fig. 11.[25,33] Another form of the fundamental Fourier components a_1 and b_1 can be obtained by the quadrature signal and the in-phase signal resulting from the lock-in amplifier, respectively. In this work, we measure the thermal diffusivity from the funda-

TABLE I. Comparison of thermal conductivities of various CVD diamonds from this work and earlier photothermal studies.

Growth process	Thickness (μm)	Diffusivity ($cm^2\,s^{-1}$)	Conductivity ($W\,cm^{-1}\,K^{-1}$)	Method	Reference
Hot-filament CVD	240	4.47	8.02 (boxcar)	time-domain PTR	This work
		4.80	8.62 (lock-in)		
	741	4.93	8.85 (boxcar)		
		4.77	8.56 (lock-in)		
	240	3.06	5.5	frequency-domain PTR	18
	450	4.85	8.7		17
Microwave plasma-enhanced CVD	16	8.10	14.68 (Phase)	spatial temperature distribution	19
		7.46	13.50 (Amp.)		
	32	7.57	13.70 (Phase)		
		7.33	13.28 (Amp.)		
	7–30	5.57	10	thermometry	20
dc plasma CVD	2000	4.46	8	unknown	36

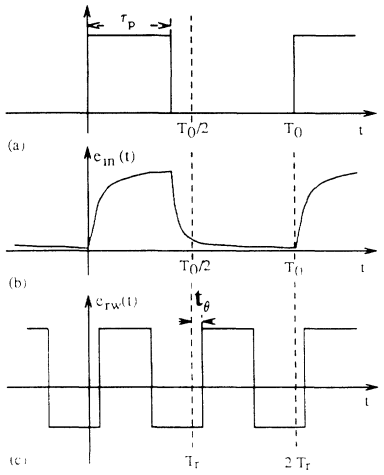

FIG. 11. Scanning lock-in photothermal rate-window principle: (a) Heating laser pulse. (b) IR radiometric photothermal transient repetition period T_0. (c) Reference signal of lock-in amplifier of period T_r, and time offset t_θ for setting the rate window.

mental Fourier component of b_1.

Because of the weighting function in the lock-in amplifier technique, both thermal buildup and decay transients must be taken into consideration in the analysis. Besides, in the lock-in rate-window method the scanning of the rate window is performed by changing the period of the repetitive heating pulse. In the case of a diamond film where the thermal transient is very fast, the pulse repetition period may extend to the range of $T_0/\tau_p \approx 1$. When T_0/τ_p approaches 1, the effect of earlier heating pulses cannot be ignored. Assuming linear superposition, here we take the effects of earlier pulses into consideration by writing

$$S_B(t)=\begin{cases}\sum_{k=0}^{N} J(t+kT_0)\ , & t\le\tau_p \\ \sum_{k=0}^{N}\left[J(t+kT_0)-J(t-\tau_p+kT_0)\right]\ , & t\ge\tau_p\ .\end{cases} \tag{20}$$

From our experience, the superposition of just two pulses prior to the current pulse will give reasonable agreement with the data. We must point out here that this is only a simplified approach. A more rigorous, but complicated and unnecessary for this experimental condition approach involves solving the thermal diffusion equations (1) with proper periodic initial conditions to find the exact solution.

One can, in principle, find the maximum position of the lock-in rate-window signal from the partial derivative $\partial b_1/\partial T_0$. Figure 12 is the theoretical prediction of the locus of maximum positions of the lock-in rate-window signal versus the characteristic time constant τ_α for samples with $\beta d = 1.3$. In Fig. 12(a), the pulse duration used in the calculation is 0.02 ms, and in Fig. 12(b) τ_p is 0.1

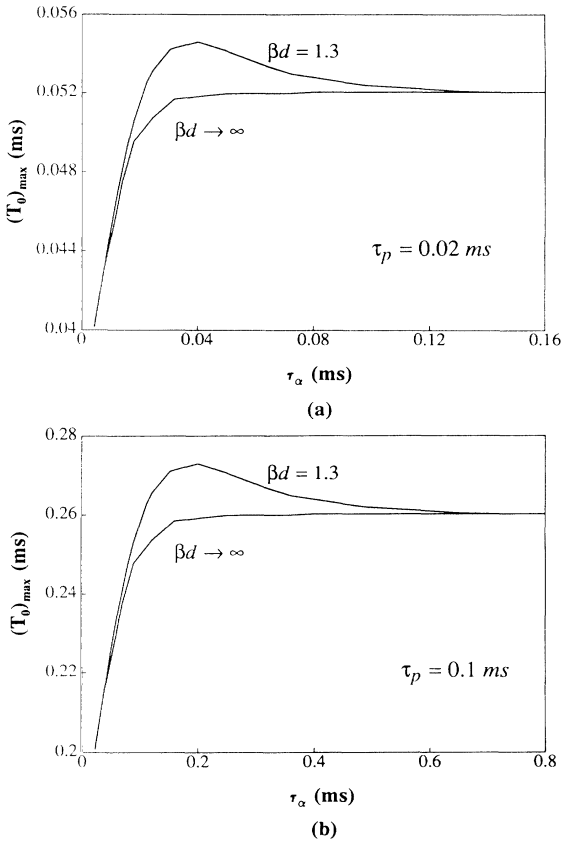

FIG. 12. Lock-in rate-window maximum $(T_0)_{max}$ vs characteristic time constant τ_α. (a) $\tau_p = 0.02$ ms. (b) $\tau_p = 0.1$ ms.

ms. Shown in Fig. 12(b) is also the theoretical prediction for the case of $\beta d \to \infty$.

Analogous to the situation in Figs. 7 and 8, in the range $0 < \tau_\alpha < \tau_p$ the relation of maximum position $(T_0)_{max}$ and the time constant is almost linear, approximated by

$$(T_0)_{max} \cong 0.88\tau_p + 0.036\ (\text{ms})\ , \quad \tau_\alpha \in [0, \tau_p] \tag{21a}$$

for $\tau_p = 0.02$ ms; and

$$(T_0)_{max} \cong 0.88\tau_p + 0.18\ (\text{ms})\ , \quad \tau_\alpha \in [0, \tau_p] \tag{21b}$$

for $\tau_p = 0.10$ ms. Compared to the boxcar rate-window method, the maximum position in the lock-in rate-window method is more sensitive to the thermal transit time constant of condensed phase materials. Similarly to the boxcar rate-window method, the longer the pulse duration, the larger the range of time constants the lock-in technique can measure and the better the S/N ratio.

Figure 13 shows the experimental photothermal lock-in rate-window signals from the CVD diamond samples. Shown in Fig. 13(a) is the result for the diamond sample D-1 and heating pulse duration 0.02 ms, and Fig. 13(b) is the result for the diamond sample D-2 and heating pulse duration 0.1 ms. From the maximum positions, the thermal diffusivities are found to be 4.80 and 4.77 cm^2/s, respectively. The corresponding calculated conductivi-

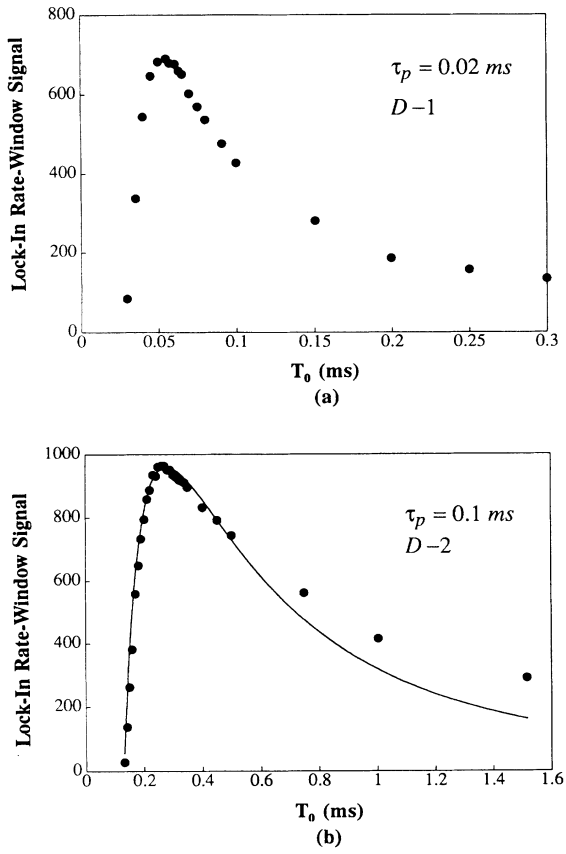

FIG. 13. Lock-in rate-window signals of CVD diamonds. (a) Diamond D-1; $L=240$ μm, $\tau_p=0.02$ ms. (b) Diamond D-2; $L=741$ μm, $\tau_p=0.1$ ms. Solid line is the theoretical result calculated by substituting the measured thermal-diffusivity value into Eqs. (10) and (18b).

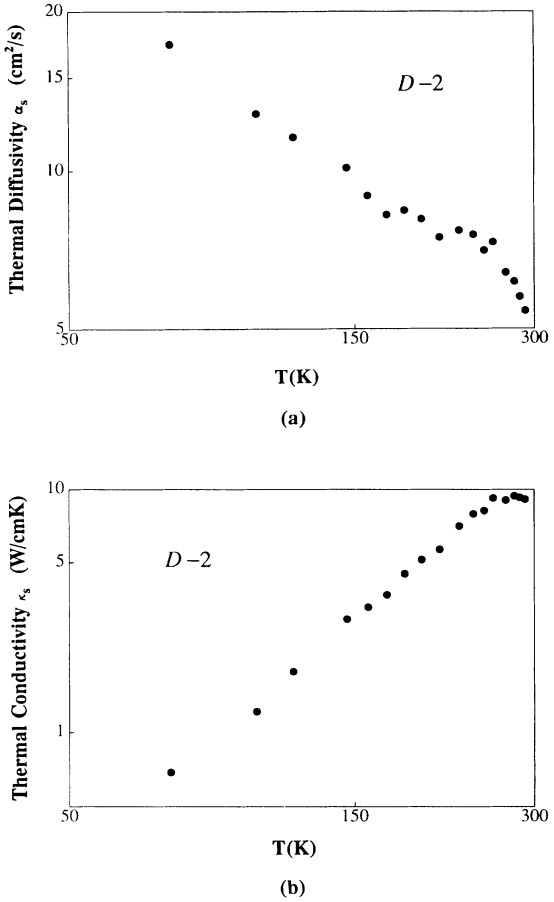

FIG. 14. Temperature dependence of thermal diffusivity (a) and thermal conductivity (b) of CVD diamond D-2.

ties are therefore found to be 8.62 and 8.56 W cm^{-1} K^{-1}, respectively. The solid line in Fig. 13(b) shows the theoretical result calculated by substituting the measured thermal-diffusivity value into Eq. (10) and then into Eq. (20). The theoretical prediction agrees with the experimental results very well in the short pulse period region but departs from the experimental results when the pulse period becomes longer. The explanation for this disagreement in the long pulse period region will be given in the next section.

V. TEMPERATURE DEPENDENCE OF THERMAL CONDUCTIVITY

Figures 14(a) and 14(b) show the thermal diffusivity and thermal conductivity, respectively, of the diamond sample D-2 from 63 K to room temperature obtained via the lock-in rate-window method. The thermal conductivity of bulk crystalline type-IIb diamond shows a peak at about 80 K,[37] but the thermal conductivity of our hot-filament-assisted CVD diamond increases monotonically with temperature and shows a peak at a much higher temperature. Our results are similar to those reported by Morelli, Beetz, and Perry measured using a steady-state four-probe technique for thin hot-filament-grown CVD diamond films.[21] The shift of the peak in the thermal conductivity toward higher temperature relative to single-crystal diamond, as well as the similarity of our room-temperature conductivity values to that of polycrystalline diamond,[32] are considered to be related to the relatively small crystallite sizes (on the order of a few μm) and the non-sp^3-carbon bonds, perhaps due to impurity incorporation in the lattice, such as sp^2 hybridized carbon,[38] as identified from the broad peak in the range 1510–1580 cm^{-1} of the Raman spectra.[21,34]

It must be remembered that the crystallite sizes are not uniform in a synthesized CVD diamond, and that they increase with the growth of the sample.[35] The surface close to the growth substrate has the smallest crystallite size and the surface far from the substrate has the largest one. As the thermal conductivity is related to the crystallite sizes, a thick CVD diamond sample should show a varying depth profile of thermal conductivity. The thermal conductivity on the side close to the growth substrate should approach that of a thin film, and the thermal conductivity on the side far from the substrate should show behavior similar to that of single-crystal diamond. Our diamond sample D-2 is relatively thick ($L=741$ μm), but the thermal conductivity shown in Fig. 14(b) shows simi-

larity to thin films. This can be explained as follows. The measurements were conducted from the smooth surface, which is the surface close to the substrate. Therefore the maximum of the rate-window signal is significantly contributed from the early portion of the thermal decay. The measured signal mainly originates in the thin layer closest to the surface, which largely resembles polycrystalline diamond, as reflected in the values of thermal conductivity calculated in Fig. 14(b). The nonuniform size crystal structure in the CVD diamonds, which is not considered in our theory, contributes to the disagreement of theory and experiment in the long pulse period region in Fig. 13(b).

VI. COMPARISON OF THE TWO PHOTOTHERMAL RATE-WINDOW SPECTROMETRIES

In this section we compare the two different photothermal rate-window spectrometries introduced in this work. Both boxcar averager and lock-in amplifier are employed to set rate windows. Since they represent different weighting functions, it is no surprise that their features are very different.

For any thermal transient, except those excited by an ideal δ-function-like pulse, the thermal buildup portion cannot be simply ignored. For simplicity, a weighting function that has both zero value and zero slope during the thermal buildup transient is preferable. From this point of view, the boxcar method shows an advantage over the lock-in amplifier method. By introducing an adjustable delay between the onset of the heating pulse and the turn on of gates at t_1 and t_2, the boxcar method can totally eliminate the effect of the thermal buildup transient and operates only on the thermal decay transient. This operation is not available with lock-in amplifiers. As shown in Sec. IV, the lock-in amplifier method is sensitive not only to the thermal transient buildup, but also to the effects of prior pulses when the pulse period approaches the pulse duration. This makes the boxcar method more suitable for cases where high S/N ratio transients can be obtained.

On the other hand, the lock-in amplifier method has superior performance from the point of view of S/N ratio. As shown in Fig. 9(a), when the transient is very noisy, the rate-window signal produced by the boxcar averager can only be reasonably calculated from the *smoothed* transient. Theoretically, the S/N ratio for any filtering operation which involves an input signal $e_{\rm in}(t)$ and a weighting function $e_{\rm RW}(t)$ is given by[24]

$$(S/N)_{\rm filter}=\frac{\int_0^{T_0} e_{\rm in}(t)e_{\rm RW}(t)dt}{\int_0^{T_0} e_{\rm RW}^2(t)dt} \tag{22}$$

in the case of a simple exponential decay

$$e_{\rm in}(t,\tau)=e^{-t/\tau} \tag{23}$$

weighted by the lock-in analyzer function $e_{\rm RW}(t,T_0)$ shown in Fig. 5, Eq. (22) gives

$$(S/N)_{\text{lock-in}}=R(1-e^{-1/2R})^2 , \tag{24}$$

where

$$R\equiv\tau/T_0 .$$

Equation (24) has a maximum for $R=R_m=0.398$, which is given by

$$[(S/N)_{\text{lock-in}}]_{\max}=\frac{R_m}{(1+R_m)^2}=0.204 . \tag{25}$$

When the boxcar weighting function $e_{\rm RW}(t,t_1,t_2)$ in Fig. 5 is considered, the relevant quantity becomes

$$(S/N)_{\rm boxcar}=\frac{\tau}{2\Delta}e^{-t_1/\tau}(1-e^{-\Delta/\tau})[1-e^{-(m-1)t_1/\tau}] , \tag{26}$$

where

$$t_2/t_1=m=\text{const}$$

and Δ is the gate width of boxcar at t_1 and t_2. In practice, $\Delta\ll t_1,\tau$, so that

$$(S/N)_{\rm boxcar}\simeq\tfrac{1}{2}e^{-1/R'}[1-e^{-(m-1)/R'}] , \tag{27}$$

where

$$R'=\tau/t_1 .$$

Equation (27) has a maximum for

$$R'=R_m=\frac{m-1}{\ln(m)}=1.442 \quad \text{if } m=2 .$$

The value of the S/N ratio when t_1 is adjusted to yield the maximum condition is ($m=2$)

$$[(S/N)_{\rm boxcar}]_{\max}=0.125 . \tag{28}$$

Therefore, for the simple case of an exponential decay, the boxcar S/N ratio is worse than that of the lock in, however, it approaches monotonically the value 0.204 in Eq. (25) as the gate width Δ of the boxcar at t_1 and t_2 increases towards $T_0/2$. This can be readily verified by setting $t_1=0$, $\Delta=t_2=T_0/2$ in Eq. (26), in which case Eq. (24) is retrieved. A similar quantitative statement concerning the S/N ratio of the two detection techniques was previously made by Miller, Ramirez, and Robinson.[24] Although one can always increase the S/N ratio of the boxcar rate window by increasing the gate width Δ at t_1 and t_2, the increase introduces significant shift in the maximum position $(t_1)_{\max}$. For fixed t_2/t_1 operation, the error in the measured $(t_1)_{\max}$ could increase up to 10% when $\Delta/(t_2-t_1)$ approaches unity.[33] Figure 15 shows two thermal transients measured from diamond sample D-2 with pulse duration 0.1 ms. In Fig. 15(a), the power of the heating pulse is 0.34 W and in Fig. 15(b) the power is only 0.025 W. Figure 16 shows the lock-in rate-window signals measured from the sample. The results with full circles were measured with heating laser power 0.025 W, and the curve with open circles corresponds to heating power of only 0.005 W. Comparing the transient shown in Fig. 15(b) and the curve with full circles in Fig. 16, one can easily assess the superiority of the lock-in amplifier method with respect to the high S/N ratio.

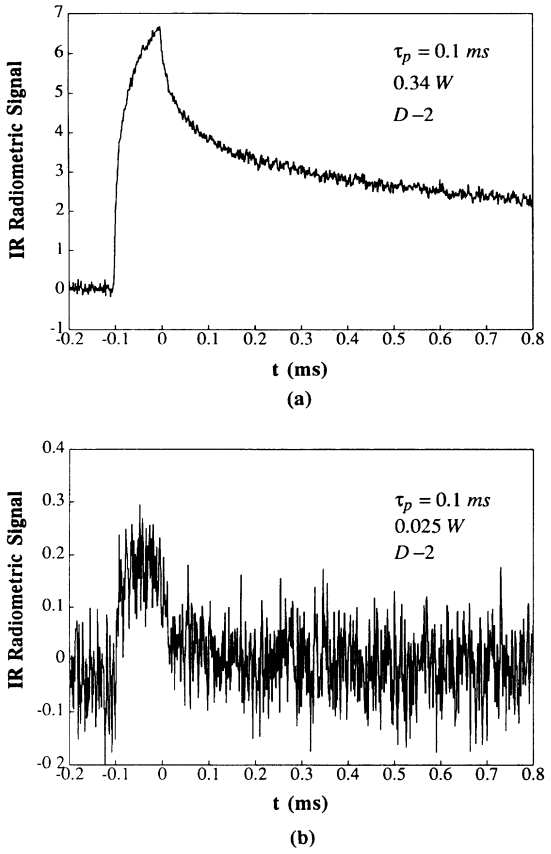

FIG. 15. Backscattered IR radiometric signals of CVD diamond D-2 with $\tau_p = 0.1$ ms. (a) Heating laser power of 0.34 W. (b) Heating laser power of 0.025 W.

The same comment applies to the other curve in Fig. 16 despite the fact that no discernible transient could be registered in the transient scope, even after the coaddition and averaging of several thousand transients. Even with the much weaker heating source (open squares with power 0.005 W), no significant shift of $(T_0)_{\max}$ can be identified from the measurement results. These facts demonstrate clearly the advantage of the lock-in amplifier

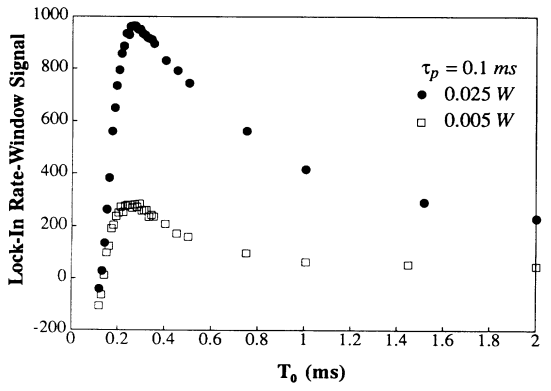

FIG. 16. Lock-in rate-window signals of CVD diamond sample D-2 with two heating laser powers. $\tau_p = 0.1$ ms.

method over the boxcar method for the measurement of weak transient signals. It is only through the use of the lock-in technique that the very low S/N ratio, low-temperature signals in Fig. 14 were able to be measured, considering the dramatic decrease of the PTR signal with T_a^3 [see Eq. (8)].

Furthermore, the lock-in amplifier method is more sensitive to the thermal transit time constant than the boxcar method. A 1% change in time constant τ_α will cause 0.6% change in the maximum position of $(t_1)_{\max}$ in the boxcar method, but will cause 0.88% change of maximum position of $(T_0)_{\max}$ in the lock-in amplifier method.

VII. SUMMARY AND CONCLUSION

Photothermal scanning rate-window spectrometry has been introduced, analyzed, and applied to hot-filament-assisted CVD diamonds. The new technique, which uses the concept of the rate window, is basically a derivative operation method for measuring the decay time constant of a thermal transient. By matching the instrumentally set rate window to the decay time constant of the transient through scanning, one measures with high precision the thermal diffusivity of the sample from the maximum of the resulting rate-window signal. The maximum position of the rate-window signal is very sensitive to the thermophysical properties of the sample because of the derivative nature of the method. The technique is a time-domain transient measurement method which extracts thermal diffusivity from the early portion of a transient. This makes the technique advantageous over time-consuming conventional frequency-domain photothermal measurement methods for the measurement of thin condensed phase samples with ultrahigh thermal diffusivity, such as diamond.

The definite advantage of the photothermal radiometric method is the nonintrusive, remote nature of this technique. The introduction of the scanning rate-window spectrometry, and comparison of the two embodiments of this technique (boxcar averager and lock-in analyzer) has been given. The boxcar rate-window spectrometry works only on the thermal transient decay of high S/N ratio signals, while the lock-in technique needs to take the thermal buildup of the transient and the effects of prior pulses into consideration. Therefore the analysis for the boxcar method is easier computationally than that for the lock-in method, but the latter gives superior S/N ratio even with transients totally embedded in the noise. The speed, sensitivity, noncontact nature, and ease of analysis make the PTR rate-window spectrometry a preferred practical method for thermal-diffusivity measurements in ultrahigh thermal conductors.

A comprehensive study of the thermal diffusivity and thermal conductivity of hot-filament CVD diamonds by using the lock-in PTR rate-window spectrometry has been given. The measured thermal conductivities of two CVD diamond samples at room temperature are 8.02 and 8.85 $\mathrm{W\,cm^{-1}\,K^{-1}}$, respectively. The results are consistent with the reported values measured using frequency-domain photothermal radiometry. The advan-

tageous features of lock-in rate-window PTR allowed the photothermal measurement of the temperature dependence of the thermal conductivity of a hot-filament-assisted CVD diamond down to 63 K without major thermal disturbance of the sample from high-fluence pulsed laser sources. The measurement was performed from the surface close to the growth substrate, and shows behavior similar to that of thin diamond films with possible incorporation of sp^2 hybridized carbon impurity into the mainly sp^3-bonded diamond lattice.

ACKNOWLEDGMENTS

The support of the Ontario Laser and Lightwave Research Center (OLLRC) and of the National Sciences and Engineering Research Council of Canada (NSERC) is gratefully acknowledged. We wish to thank Dr. Philip G. Kosky, Advanced Inorganic Materials Laboratory, General Electric Co., Schenectady, NY for supplying the diamond samples.

[1]W. J. Parker, R. J. Jenkins, C. P. Butler, and G. L. Abbott, J. Appl. Phys. **32**, 1679 (1961).

[2]D. L. Balageas, High Temp. High Pressures **21**, 85 (1989).

[3]P. K. John, L. C. M. Miranda, and A. C. Rastogi, Phys. Rev. B **34**, 4342 (1986).

[4]S. B. Peralta, Z. H. Chen, and A. Mandelis, Appl. Phys. A **52**, 289 (1991).

[5]S. B. Peralta, Z. H. Chen, and A. Mandelis, Ferroelectrics **118**, 425 (1991).

[6]S. O. Kanstad and P. E. Nordal, Powder Technol. **22**, 133 (1978).

[7]P. E. Nordal and S. O. Kanstad, Phys. Scr. **20**, 659 (1979).

[8]R. Santos and L. C. M. Miranda, J. Appl. Phys. **52**, 4192 (1981).

[9]R. D. Tom, E. P. O'Hara, and D. Benin, J. Appl. Phys. **53**, 5392 (1982).

[10]W. P. Leung and A. C. Tam, J. Appl. Phys. **56**, 153 (1984).

[11]A. C. Boccara, D. Fournier, and J. Badoz, Appl. Phys. Lett. **36**, 130 (1980).

[12]W. B. Jackson, N. M. Amer, A. C. Boccara, and D. Fournier, Appl. Opt. **20**, 1333 (1981).

[13]L. C. Aamodt and J. C. Murphy, J. Appl. Phys. **54**, 581 (1983).

[14]P. K. Kuo, M. J. Lin, C. B. Reyes, L. D. Favro, R. L. Thomas, D. S. Kim, S. Y. Zhang, L. J. Inglehart, D. Fournier, A. C. Boccara, and N. Yacoubi, Can. J. Phys. **64**, 1165 (1986).

[15]P. K. Kuo, E. D. Sendler, L. D. Favro, and R. L. Thomas, Can. J. Phys. **64**, 1168 (1986).

[16]T. R. Anthony, W. F. Banholzer, J. F. Fleischer, L. H. Wei, P. K. Kuo, R. L. Thomas, and R. W. Pryor, Phys. Rev. B **42**, 1104 (1990).

[17]A. Feldman, H. P. R. Frederikse, and X. T. Ying, Proc. SPIE **1146**, 78 (1989).

[18]A. Feldman, H. P. R. Frederikse, and S. J. Norton, Proc. SPIE J. **1325**, 304 (1990).

[19]S. Albin, W. P. Winfree, and B. S. Crews, J. Electrochem. Soc. **137**, 1973 (1990).

[20]A. Ono, T. Baba, H. Funamoto, and A. Nishikawa, Jpn. J. Appl. Phys. **25**, 808 (1986).

[21]D. T. Morelli, C. P. Beetz, and T. A. Perry, J. Appl. Phys. **64**, 3063 (1988).

[22]D. V. Lang, J. Appl. Phys. **45**, 3023 (1974).

[23]L. C. Kimerling, IEEE Trans. Nucl. Sci. NS-**23**, 1497 (1976).

[24]G. L. Miller, J. V. Ramirez, and D. A. H. Robinson, J. Appl. Phys. **46**, 2638 (1975).

[25]A. Mandelis and Z. H. Chen, Rev. Sci. Instrum. **63**, 2977 (1992).

[26]Z. H. Chen and A. Mandelis, Appl. Phys. Lett. **59**, 1 (1991).

[27]L. C. M. Miranda, Appl. Opt. **21**, 2923 (1982).

[28]I. Little, G. M. Crean, and S. J. Sheard, Mater. Sci. Eng. B **5**, 89 (1990).

[29]S. J. Sheard, M. G. Somekh, and T. Hiller, Mater. Sci. Eng. B **5**, 101 (1990).

[30]P. K. Bachmann and R. Messier, Chem. Eng. News **67**, 24 (1989).

[31]*American Institute of Physics Handbook,* edited by D. E. Gray (McGraw-Hill, New York, 1972).

[32]R. W. Pryor, P. K. Kuo, L. Wei, R. L. Thomas, and P. L. Tally, in *Diamond, Boron Nitride, Silicon Carbide and Related Wide Bandgap Semiconductors,* edited by J. T. Glass, R. F. Messier, and N. Fujimori, MRS Symposia Proceedings No. 162 (Materials Research Society, Pittsburgh, 1990), p. 273.

[33]D. S. May, M. Y. Tsai, B. G. Streetman, and D. V. Lang, J. Appl. Phys. **50**, 5093 (1979).

[34]E. N. Farabaugh, A. Feldman, and L. H. Robins, Proc. SPIE **969**, 24 (1988).

[35]P. Klocek, J. Hoggins, P. Taborek, and T. McKenna, Proc. SPIE **1325**, 63 (1990).

[36]M. Kawarada, K. Kurihara, K. Sasaki, A. Teshima, and K. Koshino, Proc. SPIE **1146**, 28 (1989).

[37]R. Berman, E. L. Foster, and J. M. Ziman, Proc. R. Soc. London, Ser. A **237**, 344 (1956).

[38]D. Beeman, J. Silverman, R. Lynds, and M. R. Anderson, Phys. Rev. B **30**, 870 (1984).